

A Study of Compact Radio Sources in Nearby Face-on Spiral Galaxies. I. Long Term Evolution of M83

L.A. Maddox^a, J.J. Cowan^a, R.E. Kilgard^b, C.K. Lacey^c, A.H. Prestwich^b, C.J. Stockdale^d,
E. Wolfing^{e,f}

ABSTRACT

We present analyses of deep radio observations of M83 taken with the Very Large Array spanning fifteen years, including never before published observations from 1990 and 1998. We report on the evolution of 55 individual point sources, which include four of the six known historical supernovae in this galaxy. A total of 10 sources have X-ray counterparts from a *Chandra* survey. Each of these sources show non-thermal spectral indices, and most appear to be X-ray supernova remnants. Comparing the radio source list to surveys in optical and X-ray, we identify three optical/X-ray supernova remnants. Nearly half of the detected radio sources in these observations are coincident with known HII regions lying in the spiral arm structures of the galaxy. We also report on changes in emission from the complex nuclear region, which has shown variability at 20cm wavelengths. We confirm that the peak radio emission from the nucleus is not coincident with the known optical center. One lesser nuclear peak is consistent with the optical/IR nucleus. Previous dynamical studies of a “dark” nuclear mass indicate a possible match to other radio nuclear emission regions in M83.

Subject headings: GALAXIES: INDIVIDUAL: (NGC 5236 = M83)—H II REGIONS—RADIO CONTINUUM: GALAXIES—SUPERNOVA REMNANTS—X-RAYS: GALAXIES

^aThe Homer L. Dodge Department of Physics and Astronomy, The University of Oklahoma, 440 W. Brooks St., Norman, OK 73019

^bHarvard-Smithsonian Center for Astrophysics, 60 Garden St, Cambridge, MA, 02138

^cDepartment of Physics and Astronomy, The University of South Carolina, 712 Main St., Columbia, SC 29208

^dDepartment of Physics, Marquette University, P.O. Box 1881, Milwaukee, WI 53201

^eDepartment of Physics and Engineering, Washington & Lee University, Lexington, VA 24450

^f Current Address: Directed Technologies Inc., 3601 Wilson Blvd., Suite 650, Arlington, VA 22201

1. Introduction

M83 (NGC 5236) is a nearby SABc galaxy that is nearly face-on ($i = 24^\circ$, Talbot et al. 1979). It is relatively nearby with distance estimates ranging from 3.75 Mpc (de Vaucouleurs 1979) to 8.9 Mpc (Sandage & Tammann 1987). We have opted to use the Cepheid-established distance of 4.5 Mpc (Thim et al. 2003). The proximity of M83 has made it an ideal candidate for observations at all wavelengths. The presence of large quantities of gas and dust imply observable levels of enhanced star formation. Previous studies have also noted vigorous star formation in the nuclear region of the galaxy (e.g., Elmegreen et al. 1998). Similar star formation activity is evidenced by the discovery of six supernovae in modern times: SN 1923A, SN 1945B, SN 1950B, SN 1957D, SN 1968L, and SN 1983N. The results of monitoring of these historical supernovae in the radio have been presented in Cowan & Branch (1982, 1985); Cowan et al. (1994); Eck et al. (1998, 2002) and Stockdale et al. (2006).

In addition to the radio surveys, several X-ray studies have been performed on M83. Kilgard et al. (2002) and Kilgard et al. (2005) included it in a larger survey of nearby galaxies. Soria & Wu (2002, 2003) also presented detailed analyses of *Chandra* observations of this galaxy. Optical surveys have also provided evidence of high star formation in the form of HII regions (Rumstay & Kaufman 1983) and supernova remnants (SNRs Blair & Long 2004).

Comparisons of compact sources at multiple wavelengths provide critical information about late stages of stellar evolution, emission mechanisms, the transition of supernovae to supernova remnants, etc. In this paper we report on the results of analysis of fifteen years of radio observations of M83, including new, never before published data from 1990 and 1998. We will begin by describing the observations dating back to 1981, before the Very Large Array¹ was completed. A brief description of the analysis techniques will then be presented in Section 3. In the sections that follow, results will be presented for specific sources. The first discussion will be a brief report on the observed historical supernovae. For the remaining unidentified sources, comparisons with optical and X-ray studies will be presented to identify SNRs, HII regions and X-ray binaries (XRBs). Finally, a discussion of the complex nuclear emission will be presented.

¹The Very Large Array of the National Radio Astronomy Observatory is a facility of the National Science Foundation operated in cooperative agreement by Associated Universities, Inc.

2. Observations and Data Reduction

We have observed M83 with the VLA several times between 1981 and 1998. Table 1 summarizes each of the observations. Reports of the 1981, 1983 and 1990 observations have been presented by Cowan & Branch (1982, 1985) and Cowan et al. (1994). The new 1998 observations will be presented here. For this paper, some of the older data have been reprocessed and reimaged in order to allow consistent analyses and comparisons over many years.

The first 20cm observation was performed on 10 April 1981 using 22 antennas while the array was being moved from A to B configuration. More 20cm observations were done on 15 and 17 December 1983 in the BnA hybrid configuration. A 6cm observation was taken on 14 March 1984 in the hybrid CnB configuration. These observations were reported in Cowan & Branch (1982, 1985) M83 was observed again at 6cm on 14 October 1990 (CnB), and at 20cm on 30 June 1990 (BnA). These were reported in Cowan et al. (1994). Finally, we observed M83 in 1998 at 20cm (June 13 and 15, BnA) and 6cm (October 31 and November 1, CnB). Cowan et al. (1994) reported results of a 1992 20 cm observation taken in B configuration. The original 1990 observation was believed to be corrupted at the time due to the dramatic fading of SN 1957D. In reprocessing this observation, we have determined it to be good, and since the array was in the preferred configuration, we have opted to present the observation here for the first time.

All of the data were processed using the Astronomical Image Processing System (AIPS) provided by NRAO. Flux calibration was performed using 3C286 as the primary source calibrator. To correct for atmospheric phase variations, a secondary calibrator, B1354-132 was used for the 1983 and 1984 observations, and J1316-336 was used for the 1990 and 1998 data sets. Due to changes in the AIPS system, we were unable to reproduce adequate maps for the earliest observations. We have opted to use the original maps presented in Cowan & Branch (1985). The remaining data were then imaged using the AIPS task IMAGR using a Briggs robustness parameter of 0. This value has the advantage of minimizing noise while allowing for excellent point source detection in resultant images. During the imaging process, we also employed self-calibration loops using the task CALIB to improve the noise levels on the maps. The data sets were deconvolved using Gaussian restoring beams, the sizes of which are indicated in Table 1. The deconvolved beams were determined using the values for the “dirty” beam, calculated from the Fourier transform of the u - v plane coverage. After imaging, the task PBCOR was run on each map to correct for the shape of the primary beam.

3. Data Analysis

An initial source list was obtained using the AIPS task SAD, which searches for points in a radio image that are higher than a specified level. A gaussian fit is the applied to each detected area of emission, and fits that fail are rejected by the algorithm. Many extended and slightly extended sources were listed as multiple sources. The list was compressed to account for this. Nuclear emission was removed from the source list. Finally, a visual inspection of the maps was performed in order to find sources that were rejected by the detection algorithm. The final list of sources along with peak flux densities at all epochs is presented in Table 2. Table 3 lists the spectral indices ($S \propto \nu^{+\alpha}$) of each source.

The sources were then fit using the AIPS task IMFIT. The input model was a two-dimensional Gaussian with a linear sloping background as was implemented in Cowan et al. (1994). Fluxes for the sources are listed in Table 2. Where no value exists, we assume a $3\text{-}\sigma$ upper limit of $0.59 \text{ mJy beam}^{-1}$ (1983 20cm), $0.14 \text{ mJy beam}^{-1}$ (1984 6cm), $0.22 \text{ mJy beam}^{-1}$ (1990 20cm), $0.11 \text{ mJy beam}^{-1}$ (1990 6cm), $0.24 \text{ mJy beam}^{-1}$ (1998 20cm), and $0.21 \text{ mJy beam}^{-1}$ (1998 6cm). The 20cm map shown in Figure 1 shows the positions of the sources in the final list. The 6cm contour map in Figure 2 indicates the positions of some of the sources discussed in Cowan et al. (1994) and Eck et al. (1998).

Many of the fluxes of the sources listed in Cowan et al. (1994) differ from fluxes listed in Table 2. The reprocessing and reimaging of the older data resulted in maps with different deconvolution sizes than those in the older maps. This produced different flux measurements than maps using the older imaging algorithms. The advantage in reprocessing lies in the fact that all of the older data have been treated in the same manner as the new data.

4. Discussion

4.1. Radio Point Sources

4.1.1. Historical Supernovae

We detected emission from four of the six historical supernovae (SNe) in M83 (SNe 1923A, 1950B, 1957D and 1983N). Source designations for each of the SNe are provided in Table 2. A more detailed discussion of the nature of the historical SNe is presented in Stockdale et al. (2006).

SN 1983N is detected only in the 1983 – 1984 observations (Cowan & Branch 1985; Cowan et al. 1994), indicating that it faded very quickly after maximum light. This is

consistent with the identification of SN 1983N as a Type Ib supernova (Weiler et al. 1986; Boffi et al. 1999).

Eck et al. (1998) reported the discovery of SN 1923A in the radio. The 1990 observations showed a very faint radio point source, and the reprocessing of the 1983 – 1984 data did hint at the presence of a source at the position of the supernova, though the flux level is too low to call it a detection. In the 1998 data, we again see a faint source that is coincident with the supernova. In the 1990 maps, the emission appears to be non-thermal in nature. Rumstay & Kaufman (1983) report the presence of an optical HII region at the position of source 59, coincident with the reported position of SN 1923A. Boffi et al. (1999) could find no optical emission consistent with a supernova expansion shock in the area around SN 1923A. It is possible that we are detecting emission from both objects, though the radio emission is near the limits of detection for the observations.

Cowan et al. (1994) and Stockdale et al. (2006) noted a continuing decline in the radio emission from SN 1957D. However there has been unusual optical activity at the position of the explosion. Long et al. (1989) reported the detection of an optical remnant of SN1957D. The remnant then faded below detectable limits within a few years (Long et al. 1992), suggesting a possible drop in the circumstellar density through which the explosion shock is propagating. Our radio observations also indicate the rapid decline of SN 1957D (see Figure 3), and the spectrum seems to be flattening. This could indicate that the supernova is approaching the level of the HII region in the area. The supernova has not faded below this level, but the flattening of the spectrum could mean a greater contribution from the thermal emission of the gas.

As reported in Stockdale et al. (2006), the radio spectrum of SN 1950B seems to have flattened and the flux has remained relatively constant across the 1990 to 1998 epochs. This would imply that the supernova has faded below the level of the local HII regions. SN 1950B occurred in a complex region of emission. Figure 4 shows the region and how the emission has changed over the course of the observations.

4.1.2. Supernova Remnants

After studying the historical supernovae, we turned our attention to searching for radio counterparts to the numerous optical SNRs reported by Blair & Long (2004). In our search we identified four sources coincident with optical SNRs. Three of these radio sources had corresponding X-ray sources as reported in Soria & Wu (2002, 2003). The SNR counterparts are listed in Table 4 and the positions are indicated in Figure 1. With the exception of source

39, all sources exhibit continuum spectral indices consistent with those due to synchrotron emission models for radio emitting SNRs (Berezhko & Völk 2004).

Source 19 is located on the edge of the southern spiral arm of M83. It has exhibited inverted spectra throughout the observations, with some flattening in 1998. The source faded at 6 cm from 1983 to 1990, and it has remained constant in flux between 1990 and 1998. It could be again that we are seeing larger contributions from thermal emission in this region. The large uncertainties in the spectral index measurements stem from the faintness of the source. Soria & Wu (2003) note the detection of a faint X-ray source coincident with source 19. Two X-ray colors are obtained: a hard color (HC), defined as $(H - M)/(H + M)$ and a soft color (SC), defined as $(M - S)/(M + S)$; where S, M and H are counts in the soft (0.3-1.0 keV), medium (1.0-2.0 keV) and hard (2.0-8.0 keV) bands, respectively. Our resulting colors ($HC = -0.19 \pm 0.45$, $SC = -0.68 \pm 0.17$) are consistent with SNR emission using the classification scheme in Prestwich et al. (2003). Our radio measurements appear to confirm the identification of this source as an SNR.

Source 22 has shown a consistent non-thermal spectrum throughout all observational epochs. It lies in the same region of the galaxy as source 19. This is a crowded region of emission along the southern spiral arm, making isolated measurements difficult. Source 22 has steepened due to the greater fading in the 6cm maps. The source has shown fairly steady emission in the 20cm band. Like source 19 there is a coincident X-ray source. Both source 19 and 22 also exhibit high $H\alpha$ luminosities (Blair & Long 2004). This is consistent with there being a denser interstellar medium in the region of the sources. The lower resolution 20 cm map presented in Cowan et al. (1994) indicates a high HI density in the area of sources 19 and 22. The X-ray colors for source 22 are not typical for an SNR ($HC = 0.15 \pm 0.22$, $SC = -0.51 \pm 0.14$), though they might indicate the presence of an XRB or an X-ray pulsar.

Source 35 has exhibited fairly steady fluxes through all epochs that we are considering. We have determined spectral indices for this source that are consistently non-thermal in nature. Our *Chandra* observations (Kilgard et al. 2005) show that this source has a very soft spectrum ($HC = -0.82 \pm 0.22$, $SC = -0.53 \pm 0.11$), indicative of SNR emission.

Source 39 differs from the other sources discussed here in that it has exhibited consistently thermal spectral indices over the time of observation. We note that the flux density of the source has remained fairly steady with some slight fading in the 6cm band. This is more consistent with the behavior of an HII region than a SNR. There is also a lack of X-ray emission from this source. Blair & Long (2004) identified the optical source as an SNR candidate based on enhanced $[SII]:H\alpha$ ratio. Further spectroscopic confirmation was not possible due to the relatively low luminosity of the region.

4.1.3. *H II Regions*

It should come as no surprise that the largest number of radio sources in M83 should be associated with HII regions. M83 is known for exhibiting vigorous star formation activity as indicated by the large number of observed SNe and SNRs. By far the largest number of optical counterparts to our radio sources do consist of HII regions. Nearly half of the reported radio sources have coincident optical sources identified with HII emission (Rumstay & Kaufman 1983). The radio/HII counterparts are listed in Table 5. It should be noted that the earlier observations represent some of the first detections of extragalactic HII in the radio at the resolution and flux level that were detected in M83. This is due in part to the depth of each observation. The deep observations also contribute to the ability to see the spiral arm structure of the galaxy as seen in Figures 1 and 2. It is in the spiral arms where HII regions would be more abundant.

It is clear from Table 5, that we are preferentially identifying large optical H II regions. Rumstay & Kaufman (1983) establish a threshold excitation parameter $U \geq 300 \text{pc cm}^{-2}$ to classify a region as large. Only 11% of the Rumstay & Kaufman (1983) sources are classified as large by this criterion, while 12 of 21 radio detected H II regions fall in this category. If the cut-off was relaxed to 250pc cm^{-2} , 19% of the Rumstay & Kaufman (1983) sources would be included, while 16 of our 21 radio detected H II regions now fall in this regime. We have restricted our comparisons to optical studies with comparable resolutions to our radio observations.

Most of the radio/optical counterpart sources show consistently stable flux densities and flat spectra indicative of thermal emission processes. This type of behavior is what would be expected from the hot gas that composes an HII region. There are notable exceptions. Source 27, although coincident with an optical HII region, is a radio lobe to a background FR II radio galaxy (Maddox et al. 2003; Soria & Wu 2003).

The spectrum of source 4 has steepened with time. It has shown a consistent increase in 20cm emission, while steadily fading at 6cm. In addition to the associated HII region, there exists an X-ray counterpart (Colbert et al. 2004). A discussion of the X-ray properties of source 4 are given in the next section.

Sources 53 and 55 are very faint sources. This leads to large uncertainties in the spectral index measurements for each of the sources. As noted earlier, source 53 is coincident with the reported optical position of SN 1923A (Eck et al. 1998). The measured flux of this source is dependent on the noise level at that position on the map. Similarly, the faint source 55 is greatly dependent on the rms map level at the position. While the emission is likely to be thermal emission from H II, we are unable to confidently identify source 55.

4.1.4. X-ray Counterparts

A comparison of our radio source list with the X-ray lists of Soria & Wu (2003) and Kilgard et al. (2005) yield 10 X-ray counterparts. These sources, along with the *Chandra* source designation, are listed in Table 6. Sources 19, 22 and 35 were discussed previously.

In order to constrain the nature of the X-ray/radio sources, we examine the X-ray colors using the values published in Kilgard et al. (2005). The X-ray color-color plot is presented in Figure 5. As can be seen, a clear dichotomy exists between X-ray binary candidates and SNR candidates: sources 3, 4, 7, 19, 22 and 35 are SNR candidates; sources 24, 32 and 36 are XRB candidates; and source 28 is a highly absorbed background source. Individual sources are discussed below. This same dichotomy between SNRs and XRBs was seen by Kilgard et al. (2006, in preparation) in M51 X-ray sources that are coincident with compact H α sources. In M51, many of the SNR-candidates are also coincident with compact radio sources. Thus, these observations help place constraints on X-ray source classification based upon X-ray colors.

Sources 3 and 4 show consistently non-thermal radio emission over the three epochs, although for source 3 we cannot calculate a spectral index due to lack of detections for at least one band in each epoch. In the radio source 3 has shown a rise in 20cm flux density from 1983 to 1990. That emission dropped to below detectability in 1998. At the same time the source brightened to a detectable level in 1998 after no detections in the two previous epochs. We do note that there are optical HII regions (Rumstay & Kaufman 1983) coincident with both radio sources. Source 3 has HC= -0.44 ± 0.31 and SC = -0.50 ± 0.15 , placing it in the range of thermal SNRs; source 4 falls on the cusp between SNRs and soft X-ray binaries (likely LMXBs), with HC= -0.57 ± 0.25 and SC= -0.22 ± 0.18 . Both sources exhibit no variability between the two *Chandra* observations.

Similarly, source 7 has X-ray colors of HC= -0.17 ± 0.27 and SC = -0.47 ± 0.15 , placing it also on the cusp of LMXBs and SNRs. Consistent non-thermal radio emission over this time strengthens the determination of this source as an SNR. There was an increase in 20cm emission, while at 6cm the flux remained flat. There is no identified optical counterpart to this source so we cannot place other constraints on the source type.

Source 24 has X-ray colors indicative of an X-ray binary, with HC = -0.20 ± 0.26 and SC= 0.11 ± 0.25 . However, the location of the source within a dust lane could lead to absorption of the soft X-rays. As such, we cannot rule out an identification of an SNR based upon the X-ray data.

Source 28 has been of particular interest since it was associated with sources 27 and 29 (Cowan et al. 1994). It was postulated that the sources could be part of a jet from the

nucleus of M83. High resolution *Chandra* observations show an X-ray source at the position of source 28. X-ray spectral analysis indicate that it is likely a background galaxy (Stockdale et al. 2001; Soria & Wu 2003). Radio observations show a source that varies slightly at 20cm while fading rapidly at 6cm. Sources 27 and 29 show consistent non-thermal emission. At 20cm source 27 has brightened slightly, while source 29 has remained steady or slightly faded (there is a large overlap in the uncertainty). Both sources faded between 1990 and 1998 at 6cm. The association of sources 27 and 29 indicate that they are the radio lobes of a FR II radio galaxy that lies along the line of sight (Stockdale et al. 2001; Maddox et al. 2003; Soria & Wu 2002, 2003).

Source 32 has the faintest X-ray detected counterpart to a radio source in M83 ($L_X < 10^{37} \text{ erg s}^{-1}$). The X-ray colors indicate that the source is a soft X-ray binary (HC= -0.73 ± 0.32 , SC = 0.00 ± 0.26). The soft X-ray color may be artificially “softened” due to excess soft, diffuse X-ray emission near the source. There is also the suggestion of X-ray variability, with the source not detected at all in the second *Chandra* observation. However, given the short observation time (20% that of the longer observation), the source would be at or slightly below the detection limit. This source lies near the confused nuclear region of the galaxy. This leads to a large background in that area. The measured spectral index for source 32 is quite steep (-1.7), but this could be attributed to the uncertainty in the background level. The source could also be exhibiting radio variability similar to the suggested X-ray variability.

Source 36 has been a mystery in previous studies. It has no optical counterpart. It is not located in the high surface brightness area of a spiral arm. The presence of the X-ray counterpart was noted first by Stockdale et al. (2001), and Maddox et al. (2003) suggested that it was another background galaxy. Radio measurements show a slight rise in 20cm emission from the earliest epoch. Over the same span of time the 6cm has dramatically dropped. Further analysis of the X-ray indicated that the source is consistent with an X-ray binary (HC= -0.13 ± 0.16 , SC= 0.15 ± 0.16), with evidence for X-ray spectral evolution between the two observations without a change in flux.

As illustrated in Figure 1 and listed in Tables 2, 4, 5, and 6, we detect radio emission from 55 point source sources overlapping with 6 X-ray only sources, 20 optical only sources, and 4 X-ray/optical sources. 54% of the sources in our radio sample have counterparts in the optical and X-ray, which can be compared to the SNR populations measured by Pannuti et al. (2002) for M33, NGC 300, and NGC 7793. For M33, they report radio emission from 53 SNRs with 37 optical and 11 optical/X-ray co-detections; for NGC 300, they report radio emission from 17 SNRs with one optical, one X-ray, and two optical/X-ray co-detections; and for NGC 7793, they report seven radio SNRs with one each optical, X-ray,

and optical/X-ray co-detection. It should be noted that the resolution for the observations was $6''$, that the statistical errors of the SNR spectral index measurements were so large that the spectral indices for most identified radio sources are not clearly identified as SNRs by their own identification ($\alpha < -0.2$), and that a large fraction of their detections would not be classified as detections in this catalog as their flux measurements do not exceed 4σ . Given these limitations, the fact that we have an approximate 50% overlap at the other bands is in relative agreement with the range of co-detections of Pannuti et al. (2002).

4.2. Nuclear Emission

The nucleus of M83 is very complex. The bright emission prevents the resolution of individual sources using the VLA configurations for the observation bands here. Cowan et al. (1994) noted that the optical/IR nucleus was not coincident with the radio nucleus. We are able to confirm this with the new analysis of the data. The peak of the radio nuclear emission is located at a distance of $\sim 10''$ from the optical center. Contour plots of all maps are shown in Figure 6.

There does exist evidence for multiple emission sources within the nuclear complex. From the 1983–1984 observations to those in 1992, there was an overall increase in the nuclear emission. Figure 7 shows a series of three dimensional emission profiles of the nuclear region. The plots for the 20cm band indicate the presence of at least four possible sources. The position of the third brightest “peak” is consistent with the optical center. Soria & Wu (2002) report the presence of a hard X-ray source at this position. X-ray spectral analysis (Soria & Wu 2002) indicate that the source is consistent with a low accretion-rate black hole with mass $\sim 10^7 M_\odot$. This compares favorably with the mass estimates of Thatte et al. (2000) ($1.6 \times 10^7 M_\odot$) and Mast et al. (2005) ($1.2 \times 10^7 M_\odot$). Although we cannot get accurate measurements of the nuclear peak flux levels in the radio maps, qualitative inspection indicates that the emission is non-thermal in nature which would be consistent with the X-ray results.

The second highest “peak” seems to be consistent with the obscured “dark” nucleus reported by Thatte et al. (2000) and subsequently studied in Sakamoto et al. (2004). In a later study, however, Mast et al. (2005) reported a different position for this “dark” nucleus. Figure 8 shows positions of the optical nucleus and the “dark” nucleus on the 1983 20cm contours. As illustrated in Figure 8 nucleus appears closer to the peak of the radio emission of the galaxy. The studies of this mass concentration indicate that it is more massive (e.g., Mast et al. 2005) than the the optical nucleus. Thatte et al. (2000) also note that the “dark” nucleus is located near the dynamical center of the galaxy. The positions of the nuclear

mass concentrations are given in Table 7. The positions for the “dark” nucleus are offset in Declination by $\sim 3.6''$, which corresponds to the deconvolution size for our observations. We would need the higher resolution of VLBI observations in order to isolate the radio emission sources.

A VLBI observation using the Long Baseline Array of the Australia Telescope has been performed on the nuclear region of M83. The aim of these observations is to resolve the individual sources in this region to get a better idea of the distribution and to find multiple counterparts to the nuclear X-ray sources reported in Soria & Wu (2003). The results of this study will be presented in a future paper (Maddox et al, in preparation).

5. Conclusions

We have studied the long term radio emission from compact sources in the galaxy M83. The observations included previously unpublished data from 1990 and 1998. We have presented the data over the fifteen years in a consistent manner. Our observations have resulted in the detection of a number of objects in M83:

- It was shown that SN 1957D has continued fading, consistent with an expanding shock through a circumstellar material that is decreasing in density. SN 1950B has apparently faded to the level of thermal HII regions that are near the position of the explosion. SN 1923A has faded to near the limits of detection of these observations. We continue to show no detection of SN 1983N after its initial radio detection, consistent with it having been a Type Ib supernova.
- About half of the radio sources are thermal HII regions. A result that is not surprising due to the high star formation activity of M83. The HII regions tend to be very large, exhibiting high excitation parameters. The largest regions are not detected due to the high resolution of our observations.
- It was found that ten sources were coincident with X-ray sources. The continuum spectral indices of these sources indicated that most were X-ray supernova remnants. We confirm that one of the coincident sources (source 28) is the nucleus of a background radio galaxy with two radio lobes (sources 27 and 29). Three of the X-ray sources are coincident with known optical supernova remnants.
- We note that the nuclear region of M83 has shown a slight increase in 20 cm emission in the radio peak. It is possible that there is an increase in accretion onto a supermassive black hole, which would be consistent with X-ray results. The 6 cm emission does not show this

increase in flux. We confirmed that the reported optical/IR nuclear peak is not consistent with the radio nucleus, though there is evidence for a radio emission region at the position of the optical nucleus. It was seen that the nuclear radio peak was near the position of a second “dark” nuclear mass concentration that corresponds to the dynamical nucleus of the galaxy.

Our multiwavelength analyses have provided new information about the nature of the many, detected compact sources and the nucleus in the starburst galaxy M83. Studies of the compact sources are providing new information about late-term stellar evolution (*e.g.*, mass-loss rates), emission mechanisms, the transition of SNe into SNRs, and the nature of XRBs. The combination of radio, X-ray and optical observations provide an excellent diagnostic for the classification of compact sources in this and other nearby galaxies. This galaxy also appears to have a complicated nuclear structure, including possibly multiple supermassive black holes, and may have minor variability. In the future we will continue to follow the long-term evolution of these sources in this galaxy, as well as to compare the results here with those in other nearby face-on spiral galaxies.

We thank the referee, A. Pedlar, for useful comments that have helped us to improve the paper. This work employed extensive use of the NASA Extragalactic Database (NED). This work was supported by NSF Grant AST-03-07279 (JJC). CJS is a Cottrell Scholar of Research Corporation and work on this project has been supported by the NASA Wisconsin Space Grant Consortium.

REFERENCES

- Berezhko, E. G., & Völk, H. J. 2004, *A&A*, 427, 525
- Blair, W. P., & Long, K. S. 2004, *ApJS*, 155, 101
- Boffi, F. R., Sparks, W. B., & Macchetto, F. D. 1999, *A&AS*, 138, 253
- Colbert, E. J. M., Heckman, T. M., Ptak, A. F., Strickland, D. K., & Weaver, K. A. 2004, *ApJ*, 602, 231
- Cowan, J. J., & Branch, D. 1982, *ApJ*, 258, 31
- . 1985, *ApJ*, 293, 400
- Cowan, J. J., Roberts, D. A., & Branch, D. 1994, *ApJ*, 434, 128
- de Vaucouleurs, G. 1979, *AJ*, 84, 1270

- de Vaucouleurs, G., Pence, W. D., & Davoust, E. 1983, *ApJS*, 53, 17
- Eck, C. R., Cowan, J. J., & Branch, D. 2002, *ApJ*, 573, 306
- Eck, C. R., Roberts, D. A., Cowan, J. J., & Branch, D. 1998, *ApJ*, 508, 664
- Elmegreen, D. M., Chromey, F. R., & Warren, A. R. 1998, *AJ*, 116, 2834
- Kilgard, R. E., et al. 2005, *ApJS*, 159, 214
- Kilgard, R. E., Kaaret, P., Krauss, M. I., Prestwich, A. H., Raley, M. T., & Zezas, A. 2002, *ApJ*, 573, 138
- Long, K. S., Blair, W. P., & Krzeminski, W. 1989, *ApJ*, 340, L25
- Long, K. S., Winkler, P. F., & Blair, W. P. 1992, *ApJ*, 395, 632
- Maddox, L. A., Stockdale, C. J., & Cowan, J. J. 2003, *BAAS*35, 1396
- Mast, D., Díaz, R. J., & Aguero, M. P. 2005, *ArXiv Astrophysics e-prints*, arXiv:astro-ph/0505264
- Pannuti, T. G., Duric, N., Lacey, C. K., Ferguson, A. M. N., Magnor, M. A., & Mendelowitz, C. 2002, *ApJ*, 565, 966
- Prestwich, A. H., Irwin, J. A., Kilgard, R. E., Krauss, M. I., Zezas, A., Primini, F., Kaaret, P., & Boroson, B. 2003, *ApJ*, 595, 719
- Rumstay, K. S., & Kaufman, M. 1983, *ApJ*, 274, 611
- Sakamoto, K., Matsushita, S., Peck, A. B., Wiedner, M. C., & Iono, D. 2004, *ApJ*, 616, L59
- Sandage, A., & Tammann, G. A. 1987, *A revised Shapley-Ames Catalog of bright galaxies* (Carnegie Institution of Washington Publication, Washington: Carnegie Institution, 1987 , 2nd ed.)
- Soria, R., & Wu, K. 2002, *A&A*, 384, 99
- . 2003, *A&A*, 410, 53
- Stockdale, C. J., et al. 2001, *BAAS*, 33, 1338
- Stockdale, C. J., Maddox, L. A., Cowan, J. J., Prestwich, A., Kilgard, R., & Immler, S. 2006, *AJ*, 131, 889

Talbot, R. J., Jensen, E. B., & Dufour, R. J. 1979, *ApJ*, 229, 91

Thatte, N., Tecza, M., & Genzel, R. 2000, *A&A*, 364, L47

Thim, F., Tammann, G. A., Saha, A., Dolphin, A., Sandage, A., Tolstoy, E., & Labhardt, L. 2003, *ApJ*, 590, 256

Weiler, K. W., Sramek, R. A., Panagia, N., van der Hulst, J. M., & Salvati, M. 1986, *ApJ*, 301, 790

Table 1. VLA RADIO OBSERVATIONS OF M83

PARAMETER	1983 – 1984 OBSERVATIONS		1990 OBSERVATIONS		1998 OBSERVATIONS	
	20cm	6cm	20cm	6cm	20cm	6cm
Frequency (GHz)	1.446	4.873	1.452	4.873	1.465	4.885
Observing dates	1983 Dec 15,17	1984 Mar 15	1990 Jun 30	1990 Oct 14	1998 Jun 13	1998 Oct 31
Observing time (hr)	3	6.5	7.5	6	11.3	11.6
Configuration	BnA	CnB	BnA	CnB	BnA	CnB
Primary beam HPBW	30'	8'	30'	8'	30'	8'
Clean Beam	3''50 × 3''50	3''93 × 2''80	3''65 × 3''65	3''65 × 3''65	3''65 × 3''65	3''65 × 3''65
rms noise (mJy beam ⁻¹)	0.197	0.045	0.074	0.037	0.079	0.070

Table 2. Radio Positions and Peak Flux Densities of Sources in M83

Source	Position ^a		1983-1984 ^b		1990		1998	
	R.A.(2000)	Decl.(2000)	20 cm (mJy)	6 cm (mJy)	20 cm (mJy)	6 cm (mJy)	20 cm (mJy)	6 cm (mJy)
1	13 ^h 36 ^m 50 ^s .00	−29°52′43″.36	...	0.41 ± 0.08	0.37 ± 0.08	0.35 ± 0.04	0.52 ± 0.07	0.34 ± 0.06
2	13 36 50.83	−29 51 59.56	0.38 ± 0.08
3	13 36 50.86	−29 52 38.54	0.76 ± 0.20	0.39 ± 0.08	0.38 ± 0.08	0.25 ± 0.03	0.40 ± 0.09	0.20 ± 0.06
4	13 36 51.11	−29 50 41.98	0.96 ± 0.19	...	0.55 ± 0.08	0.23 ± 0.04	0.58 ± 0.07	0.34 ± 0.04
5 ^c	13 36 51.24	−29 54 02.01	4.58 ± 0.20	1.30 ± 0.12
6	13 36 51.55	−29 53 00.61	0.43 ± 0.08	0.41 ± 0.05	0.54 ± 0.10	0.36 ± 0.06
7	13 36 52.78	−29 52 31.58	0.52 ± 0.08	0.25 ± 0.04	0.47 ± 0.10	0.29 ± 0.05
8	13 36 52.77	−29 51 10.39	...	0.45 ± 0.07	0.38 ± 0.08	0.49 ± 0.04	0.42 ± 0.09	0.30 ± 0.05
9	13 36 52.83	−29 51 37.96	0.62 ± 0.08	...	0.90 ± 0.08	...
10	13 36 52.91	−29 52 49.07	0.73 ± 0.19	0.39 ± 0.08	0.60 ± 0.08	0.28 ± 0.05	0.45 ± 0.09	0.28 ± 0.05
11 ^c	13 36 52.92	−29 51 56.50	0.70 ± 0.17	0.43 ± 0.06	0.54 ± 0.08	0.54 ± 0.05	0.53 ± 0.07	0.50 ± 0.04
12	13 36 53.14	−29 51 33.12	0.98 ± 0.19	1.03 ± 0.06	0.95 ± 0.08	1.16 ± 0.05	0.89 ± 0.13	1.17 ± 0.05
13	13 36 53.27	−29 52 57.44	0.47 ± 0.19	0.53 ± 0.08	0.45 ± 0.08	0.40 ± 0.06	0.60 ± 0.08	0.47 ± 0.05
14	13 36 53.25	−29 50 58.62	...	0.31 ± 0.06	0.42 ± 0.08	0.41 ± 0.04	0.20 ± 0.08	0.35 ± 0.04
15	13 36 53.39	−29 51 11.17	0.18 ± 0.04	...	0.19 ± 0.05
16	13 36 54.20	−29 50 42.22	...	0.45 ± 0.06	0.37 ± 0.08	0.30 ± 0.05	0.41 ± 0.07	0.33 ± 0.04
17	13 36 54.40	−29 53 05.17	0.43 ± 0.21	0.37 ± 0.08	0.36 ± 0.08	0.49 ± 0.05	0.52 ± 0.11	0.58 ± 0.06
18	13 36 54.74	−29 52 56.77	0.59 ± 0.19	0.47 ± 0.08	0.60 ± 0.08	0.33 ± 0.05	0.44 ± 0.10	0.29 ± 0.06
19	13 36 54.90	−29 53 10.29	...	0.58 ± 0.08	...	0.40 ± 0.04	0.36 ± 0.10	0.43 ± 0.05
20	13 36 54.95	−29 52 40.21	0.19 ± 0.05	0.28 ± 0.09	...
21	13 36 55.41	−29 52 56.08	0.26 ± 0.08	...	0.26 ± 0.09	0.21 ± 0.03
22	13 36 55.54	−29 53 03.26	0.22 ± 0.08	0.26 ± 0.04	0.33 ± 0.09	0.32 ± 0.05
23	13 36 55.72	−29 49 52.14	0.88 ± 0.18	0.51 ± 0.06	0.70 ± 0.08	0.43 ± 0.04	0.46 ± 0.06	0.53 ± 0.05
24	13 36 56.13	−29 52 54.99	0.45 ± 0.08	0.31 ± 0.04	0.42 ± 0.07	...
25	13 36 56.32	−29 49 34.10	0.13 ± 0.03	0.30 ± 0.05	...
26	13 36 56.84	−29 52 48.36	0.27 ± 0.04	0.35 ± 0.08	0.25 ± 0.04
27	13 36 56.91	−29 50 43.28	3.39 ± 0.18	0.86 ± 0.05	3.23 ± 0.08	1.09 ± 0.03	3.38 ± 0.07	1.02 ± 0.04
28	13 36 58.34	−29 51 04.58	0.74 ± 0.18	1.31 ± 0.06	1.06 ± 0.08	1.55 ± 0.04	0.82 ± 0.07	0.87 ± 0.05
29	13 36 59.00	−29 51 16.04	1.39 ± 0.21	0.37 ± 0.05	1.45 ± 0.07	0.60 ± 0.04	1.38 ± 0.07	0.49 ± 0.04
30	13 36 59.54	−29 51 26.32	0.73 ± 0.07	...	1.26 ± 0.09	...
31	13 36 59.98	−29 52 16.65	2.29 ± 0.19	1.35 ± 0.06	2.19 ± 0.08	1.45 ± 0.05	2.11 ± 0.09	1.56 ± 0.05
32	13 37 00.17	−29 51 40.02	1.75 ± 0.21	0.42 ± 0.06	2.16 ± 0.08	0.57 ± 0.03	2.85 ± 0.12	0.38 ± 0.08
33	13 37 00.54	−29 54 18.50	0.20 ± 0.08	0.27 ± 0.05
34	13 37 01.34	−29 51 26.51	1.34 ± 0.22	0.95 ± 0.05	0.92 ± 0.08	0.87 ± 0.04	1.14 ± 0.09	0.85 ± 0.04
35	13 37 02.36	−29 51 25.85	0.94 ± 0.21	...	0.77 ± 0.08	0.48 ± 0.04	0.66 ± 0.08	0.37 ± 0.05
36	13 37 03.24	−29 52 26.56	...	1.13 ± 0.06	0.50 ± 0.08	0.63 ± 0.04	0.68 ± 0.07	0.32 ± 0.04
37	13 37 03.28	−29 51 13.7	0.24 ± 0.08	0.22 ± 0.05
38	13 37 03.39	−29 54 02.04	1.01 ± 0.23	1.07 ± 0.07	0.66 ± 0.08	1.04 ± 0.05	0.80 ± 0.06	1.00 ± 0.05
39 ^c	13 37 03.53	−29 49 40.56	2.72 ± 0.21	2.18 ± 0.06	1.88 ± 0.08	1.57 ± 0.04	0.82 ± 0.09	0.60 ± 0.05
40	13 37 04.73	−29 50 57.59	...	0.32 ± 0.06	0.27 ± 0.08	0.36 ± 0.04	0.67 ± 0.08	0.41 ± 0.05
41	13 37 06.61	−29 53 32.32	...	0.75 ± 0.09	0.59 ± 0.08	0.42 ± 0.05	0.56 ± 0.08	0.31 ± 0.05
42	13 37 06.91	−29 49 36.03	1.30 ± 0.23	1.42 ± 0.05	1.51 ± 0.08	1.53 ± 0.04	1.54 ± 0.07	1.50 ± 0.05
43	13 37 07.37	−29 51 06.38	...	0.32 ± 0.06	0.27 ± 0.08	0.43 ± 0.04	0.38 ± 0.06	0.34 ± 0.05

Table 2—Continued

Source	Position ^a		1983-1984 ^b		1990		1998	
	R.A.(2000)	Decl.(2000)	20 cm (mJy)	6 cm (mJy)	20 cm (mJy)	6 cm (mJy)	20 cm (mJy)	6 cm (mJy)
44	13 37 07.40	−29 52 06.91	0.23 ± 0.08	0.20 ± 0.04
45	13 37 07.66	−29 51 13.28	0.60 ± 0.21	0.31 ± 0.06	0.55 ± 0.07	0.47 ± 0.04	0.49 ± 0.07	0.40 ± 0.06
46	13 37 07.74	−29 53 13.99	0.26 ± 0.08	0.22 ± 0.04	...	0.23 ± 0.04
47	13 37 07.82	−29 52 41.69	0.28 ± 0.08	0.26 ± 0.05	0.23 ± 0.06	...
48	13 37 07.89	−29 51 17.78	0.66 ± 0.22	0.65 ± 0.07	0.98 ± 0.07	0.53 ± 0.04	0.65 ± 0.07	0.62 ± 0.05
49	13 37 08.09	−29 52 55.78	0.34 ± 0.09	0.23 ± 0.05	0.34 ± 0.07	0.29 ± 0.05
50	13 37 08.31	−29 52 11.54	0.68 ± 0.22	0.35 ± 0.08	0.46 ± 0.09	0.41 ± 0.04	0.40 ± 0.08	0.38 ± 0.05
51	13 37 08.69	−29 51 31.04	...	0.39 ± 0.06	0.26 ± 0.08	0.31 ± 0.04	0.48 ± 0.08	0.23 ± 0.05
52	13 37 09.19	−29 51 33.31	0.86 ± 0.22	0.38 ± 0.07	0.48 ± 0.07	0.33 ± 0.04	0.70 ± 0.07	0.35 ± 0.04
53 ^c	13 37 09.22	−29 51 00.51	0.28 ± 0.04	0.22 ± 0.06	0.19 ± 0.05
54	13 37 10.01	−29 51 28.24	...	0.45 ± 0.06	...	0.20 ± 0.04	0.29 ± 0.09	0.25 ± 0.06
55	13 37 11.44	−29 49 52.31	0.23 ± 0.05	0.21 ± 0.06	0.18 ± 0.06

^aFrom 1998 6 cm observations.

^bFlux measurements using original maps discussed in Cowan & Branch (1985). Included here for completeness.

^cIn order of appearance: SN 1983N, SN 1950B, SN 1957D, and SN 1923A.

Table 3. SPECTRAL INDICES OF SOURCES IN M83

SOURCE	SPECTRAL INDEX	
	1990	1998
1	-0.05 ± 0.24	-0.36 ± 0.22
2	< -1.01	...
3	-0.35 ± 0.24	-0.58 ± 0.38
4	-0.73 ± 0.23	-0.45 ± 0.17
5
6	-0.04 ± 0.22	-0.34 ± 0.25
7	-0.61 ± 0.22	-0.41 ± 0.27
8	0.21 ± 0.23	-0.28 ± 0.27
9	< -1.42	< -1.20
10	-0.64 ± 0.22	-0.40 ± 0.27
11	0.00 ± 0.17	-0.05 ± 0.15
12	0.17 ± 0.09	0.23 ± 0.15
13	-0.10 ± 0.23	-0.21 ± 0.17
14	-0.02 ± 0.21	0.47 ± 0.42
15	> -0.17	> -0.18
16	-0.18 ± 0.27	-0.18 ± 0.21
17	0.26 ± 0.24	0.09 ± 0.24
18	-0.50 ± 0.20	-0.35 ± 0.31
19	> 0.49	0.15 ± 0.30
20	> -0.13	< -0.23
21	< -0.70	-0.18 ± 0.37
22	0.14 ± 0.39	-0.03 ± 0.31
23	-0.41 ± 0.15	0.12 ± 0.16
24	-0.31 ± 0.22	< -0.57
25	> -0.44	< -0.29
26	> 0.16	-0.28 ± 0.28
27	-0.91 ± 0.04	-1.01 ± 0.04
28	0.32 ± 0.08	0.05 ± 0.10
29	-0.74 ± 0.08	-0.87 ± 0.10
30	< -1.55	< -1.48

Table 3—Continued

SOURCE	SPECTRAL INDEX	
	1990	1998
31	-0.35 ± 0.05	-0.25 ± 0.05
32	-1.12 ± 0.06	-1.70 ± 0.21
33	0.25 ± 0.44	...
34	-0.05 ± 0.10	-0.25 ± 0.09
35	-0.40 ± 0.13	-0.49 ± 0.18
36	0.19 ± 0.17	-0.63 ± 0.16
37	< -0.64	> -0.06
38	0.38 ± 0.13	0.19 ± 0.09
39	-0.15 ± 0.05	-0.26 ± 0.14
40	0.24 ± 0.32	-0.41 ± 0.17
41	-0.28 ± 0.18	-0.50 ± 0.22
42	0.01 ± 0.06	-0.02 ± 0.06
43	0.39 ± 0.31	-0.09 ± 0.22
44	-0.12 ± 0.40	...
45	-0.13 ± 0.15	-0.17 ± 0.21
46	-0.14 ± 0.36	> -0.02
47	-0.06 ± 0.34	< -0.08
48	-0.52 ± 0.10	-0.04 ± 0.13
49	-0.33 ± 0.34	-0.13 ± 0.27
50	-0.10 ± 0.22	-0.04 ± 0.24
51	0.15 ± 0.33	-0.62 ± 0.27
52	-0.31 ± 0.19	-0.58 ± 0.15
53	> 0.19	-0.12 ± 0.38
54	> -0.09	-0.12 ± 0.39
55	> 0.03	-0.13 ± 0.44

Table 4: Optical Supernova Remnants with Radio Counterparts

Source	Radio Spectral Index	SNR
19....	$+0.15 \pm 0.30$	BL18
22....	-0.18 ± 0.37	BL24
35....	-0.49 ± 0.18	BL41
39....	-0.26 ± 0.14	BL50

Table 5: Radio Sources with Associated HII Regions

Source	Radio Spectral Index	HII Region	Excitation Parameter ^a
2	< -1.02	RK230	241
3	-0.58 ± 0.38	RK233	355
4	-0.45 ± 0.17	RK223	444
6	$+0.34 \pm 0.25$	RK292/295	228/287
8	-0.28 ± 0.27	RK211	393
12	$+0.23 \pm 0.15$	RK209	321
18 ^b	-0.35 ± 0.31
22	-0.03 ± 0.31	RK185	369
26	-0.28 ± 0.28	RK181	201
33	$+0.25 \pm 0.44$	RK144	300
34	-0.25 ± 0.09	RK137	473
37	> -0.06	RK119	97
40	-0.41 ± 0.17	RK110	470
42	-0.02 ± 0.06	RK86	316
43	-0.09 ± 0.22	RK79	288
45/48	-0.04 ± 0.13	RK75	395
46	-0.14 ± 0.36	RK78	228
49	-0.13 ± 0.27	RK73	301
50	-0.04 ± 0.24	RK70	353
53	-0.12 ± 0.38	RK59	323
55	-0.13 ± 0.44	RK37	294

^aThe excitation parameter U is a measure of the total Lyman continuum flux and is a useful index of the distribution of O stars. The values are in units of pc cm^{-2} , as presented in Rumstay & Kaufman (1983).

^bThis source was detected as an HII in a survey by de Vaucouleurs et al. (1983), listed as source 23.

Table 6: X-Ray Counterparts to Radio Sources in M83

Source	Radio Spectral Index	CXOU	Source Type	Reference
3.....	-0.58 ± 0.38	J133650.8-295240	HII Region/SNR	1
4.....	-0.45 ± 0.17	J133651.1-295043	HII Region/LMXB	1
7.....	-0.41 ± 0.27	J133652.8-295231	SNR	1
19....	$+0.15 \pm 0.30$	J133655.0-295239	SNR	2
22....	-0.02 ± 0.31	J133655.6-295303	SNR	2
24....	-0.31 ± 0.22	J133656.2-295255	...	
28....	$+0.05 \pm 0.10$	J133658.3-295105	Background Galaxy	3
32....	-1.70 ± 0.21	J133700.0-295138	...	
35....	-0.49 ± 0.18	J133702.4-295126	SNR	2
36....	-0.63 ± 0.16	J133703.3-295226	XRB	

(1) Colbert et al. (2004)

(2) Blair & Long (2004)

(3) Stockdale et al. (2001)

Table 7: REPORTED POSITIONS OF NUCLEAR MASS CONCENTRATIONS

	RA (J2000)	Dec (J2000)	Reference
Optical Nucleus	13 37 00.79	–29 51 58.60	Cowan et al. (1994)
Hidden Nucleus	13 37 00.54	–29 51 53.62	Mast et al. (2005)
	14 37 00.72	–29 51 57.20	Thatte et al. (2000)

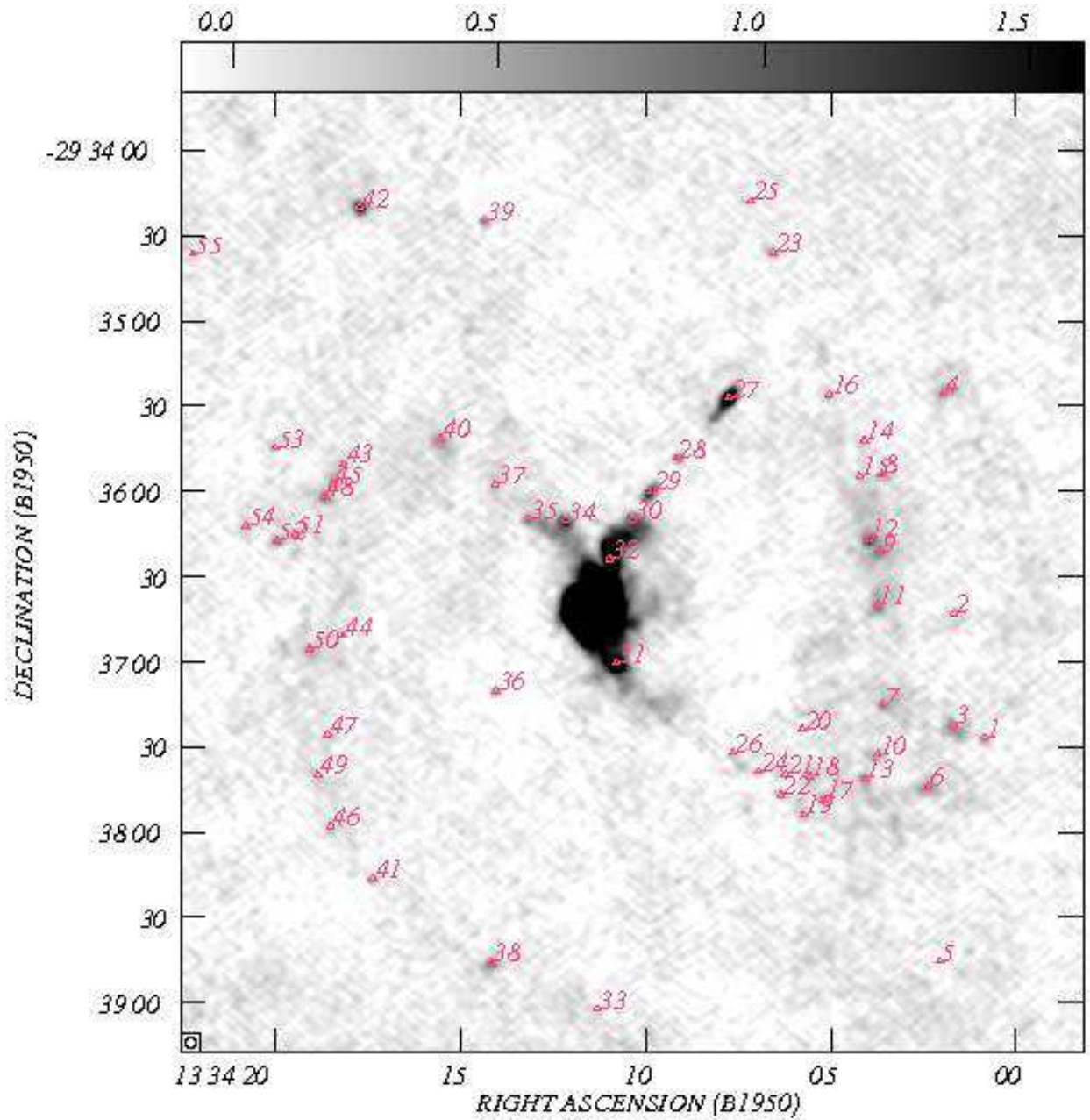


Fig. 1.— A 20cm map of M83 from the 1998 observation. Sources indicated correspond to those in Table 2. Greyscale spans from -0.1 mJy to 1.6 mJy.

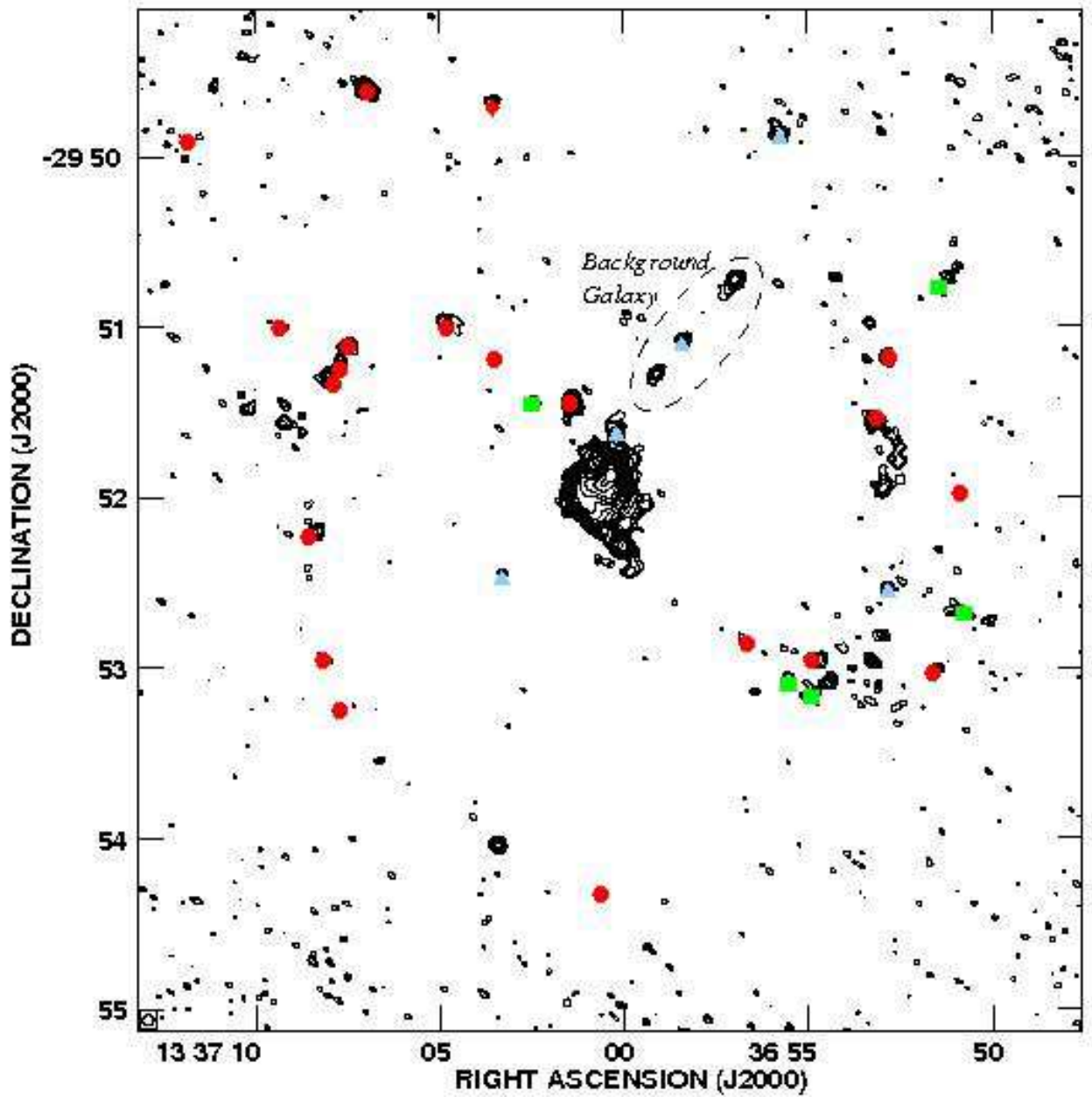


Fig. 2.— 6cm contours of M83. Red symbols indicate radio sources with optical counterparts. Red circles are HII regions, while the red diamond indicates an optical SNR. Blue triangles indicate the presence of X-ray counterparts. Green squares denote sources that have emission in radio, optical and X-ray. Contour levels are 0.14, 0.20, 0.28, 0.40, 0.57, 0.80, 1.13, 1.60, 2.26, 3.20, 4.53, 6.40, 9.05 and 12.80 mJy/beam.

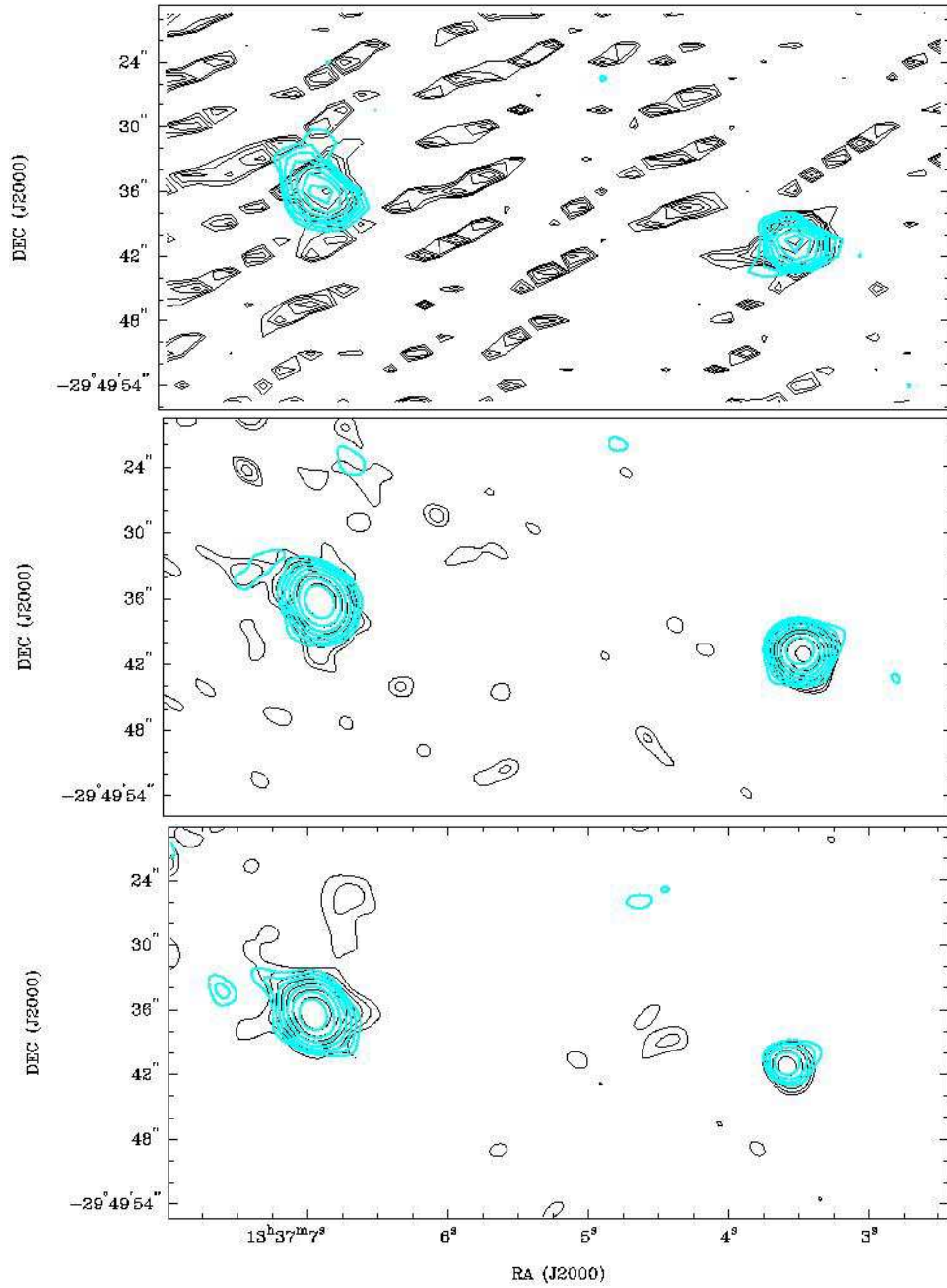


Fig. 3.— A series of contour plots showing the time evolution of SN 1957D. Black contours are 20cm emission and thick blue green contours are 6cm emission. Contour levels for both plots are 0.20, 0.28, 0.40, 0.57, 0.8, 1.13, 1.60 and 2.26 mJy/beam. SN 1957D is the right hand source. The left hand source is an HII region. Time runs from top to bottom.

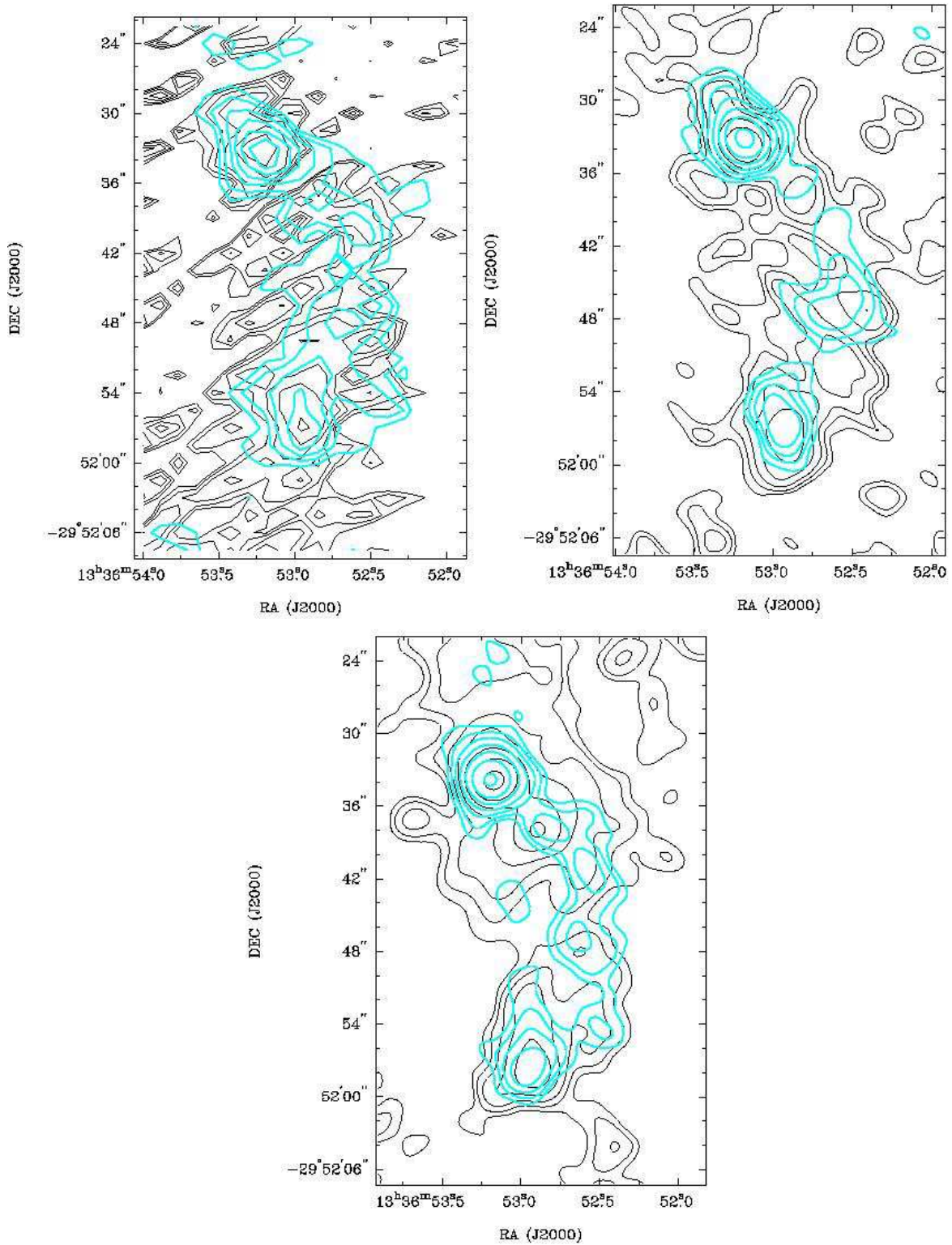


Fig. 4.— Same as Figure 3, but near the region of SN 1950B. Contour levels are the same. SN 1950B is the lower of the two major sources. Time progress clockwise from the upper left.

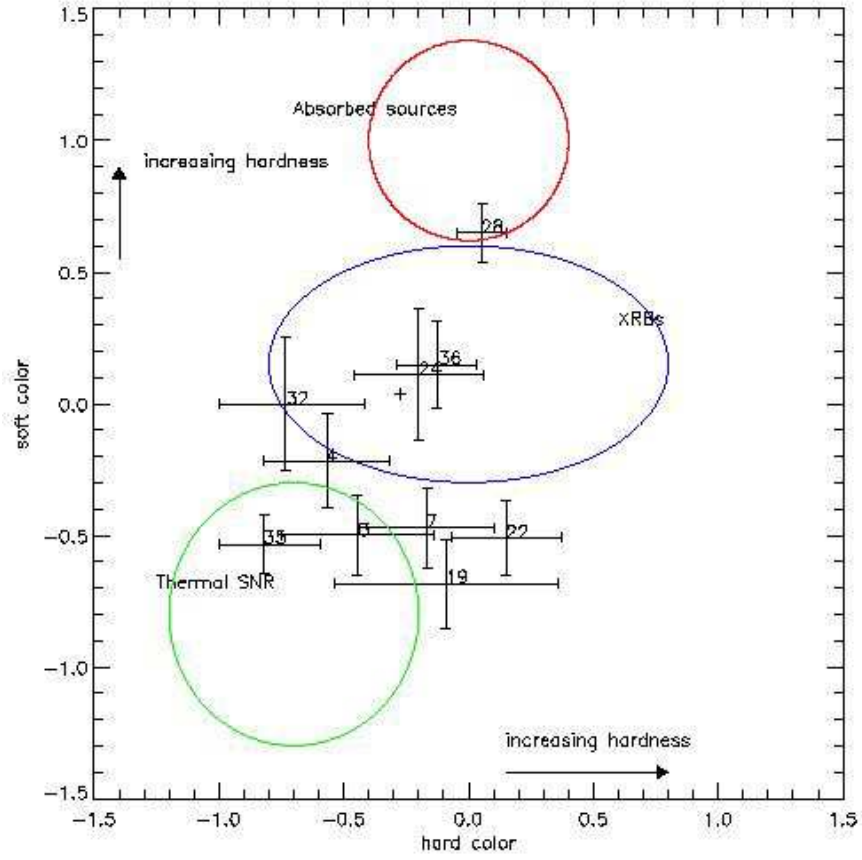


Fig. 5.— X-ray color-color diagram for the X-ray/Radio counterpart sources in M83.

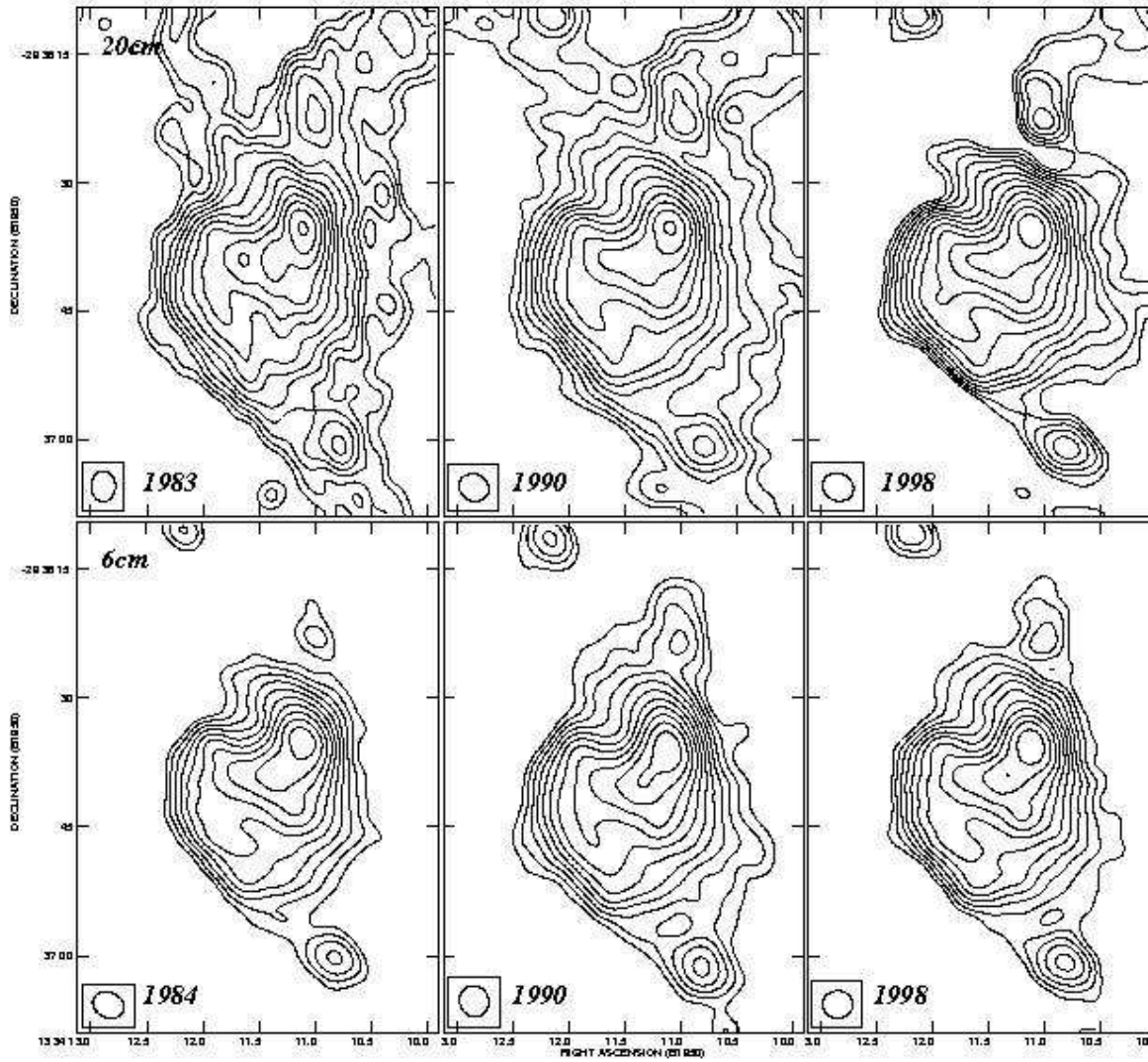


Fig. 6.— Same as Figure 3, but for the nuclear region. Contour levels are 0.40, 0.57, 0.8, 1.13, 1.60, 2.26, 3.20, 4.53, 6.40, 9.05, 12.80, 18.10 and 25.59 mJy/beam.

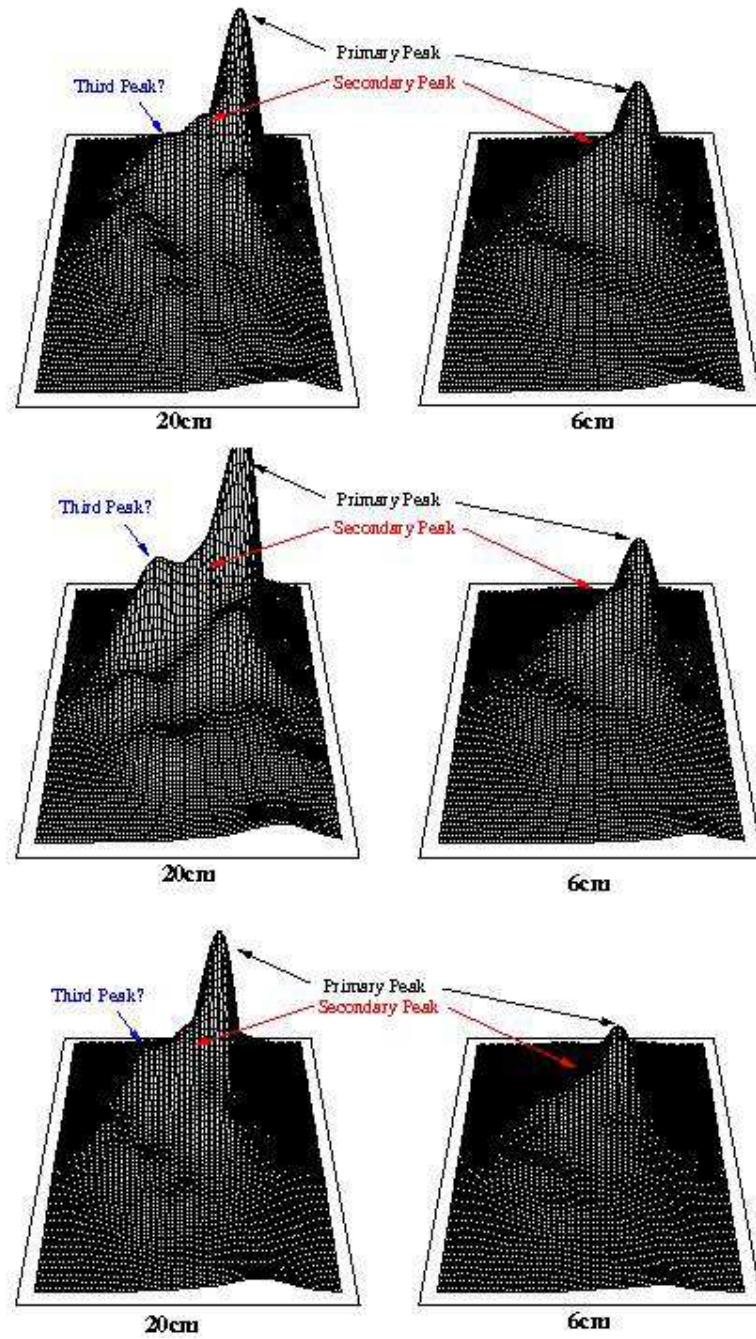


Fig. 7.— A series of profile plots of the nuclear region. Flux peaks are scaled to the 1990 20cm observation to show the differences between 20cm (left) and 6cm (right). Time progresses from top to bottom. One notable feature of these plots is the evidence for several lesser “peaks” of emission in the 20cm images.

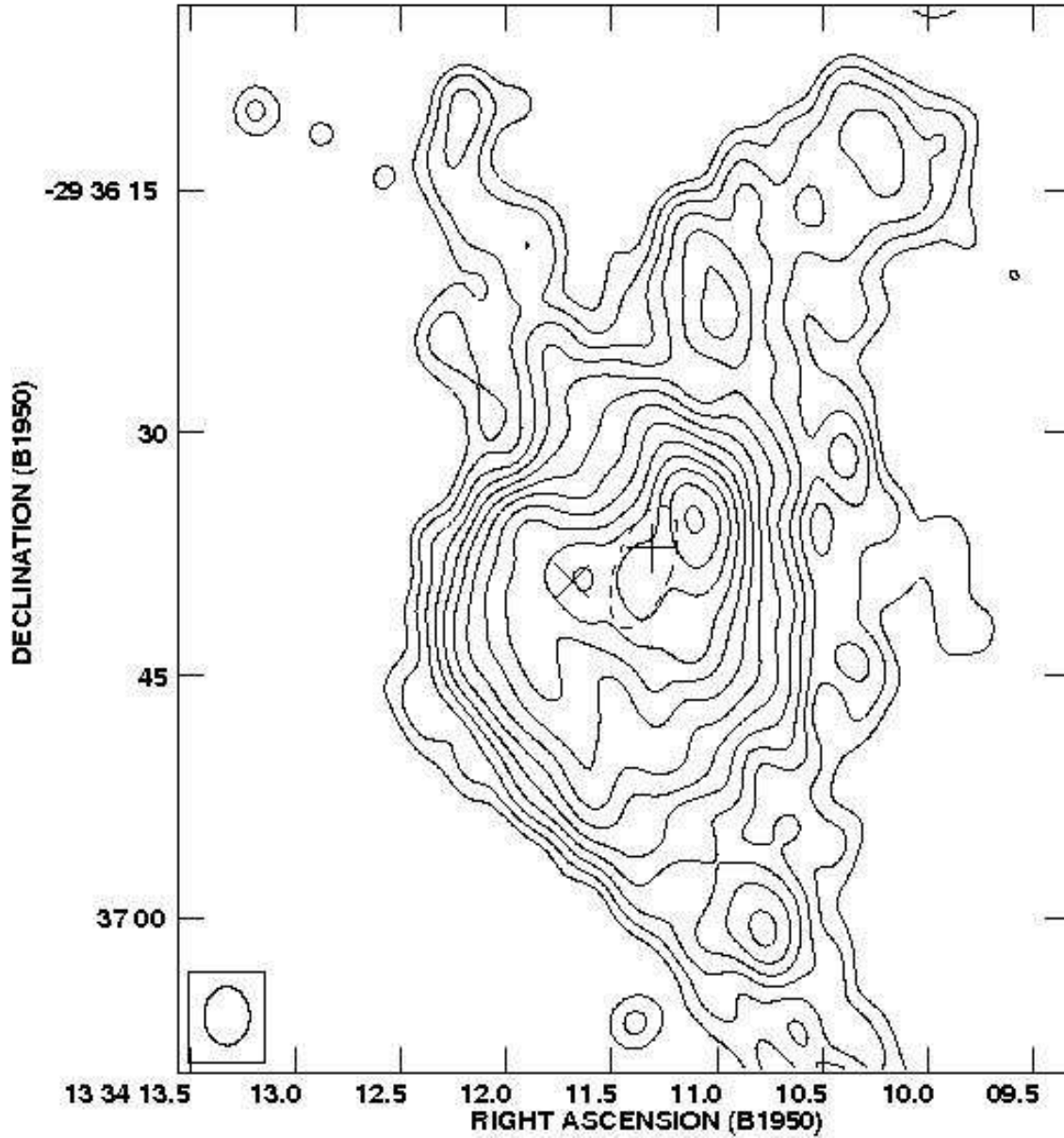


Fig. 8.— Contours of 20cm emission from the 1983 observation. Contour levels are same as Figure 6. The cross indicates the position of the optical nucleus. The plus sign indicates the reported position of the hidden nuclear mass as determined by Mast et al. (2005). The ellipse surrounding the plus indicates a probable region in which the hidden mass lies due to another estimate by Thatte et al. (2000).